Cathodoluminescence hyperspectral imaging of trench-like defects in InGaN/GaN quantum well structures

2014 J. Phys. D: Appl. Phys. 47 135107

(http://iopscience.iop.org/0022-3727/47/13/135107)

OPEN ACCESS
IOP Publishing
Journal of Physics D: Applied Physics
J. Phys. D: Appl. Phys. **47** (2014) 135107 (6pp)
doi:10.1088/0022-3727/47/13/135107

Cathodoluminescence hyperspectral imaging of trench-like defects in InGaN/GaN quantum well structures

Jochen Bruckbauer[1], Paul R Edwards[1], Suman-Lata Sahonta[2], Fabien C-P Massabuau[2], Menno J Kappers[2], Colin J Humphreys[2], Rachel A Oliver[2] and Robert W Martin[1]

[1] Department of Physics, SUPA, University of Strathclyde, Glasgow G4 0NG, UK
[2] Department of Materials Science and Metallurgy, University of Cambridge, Cambridge CB3 0FS, UK

E-mail: jochen.bruckbauer@strath.ac.uk

Received 13 January 2014, revised 5 February 2014
Accepted for publication 6 February 2014
Published 11 March 2014

Abstract

Optoelectronic devices based on the III-nitride system exhibit remarkably good optical efficiencies despite suffering from a large density of defects. In this work we use cathodoluminescence (CL) hyperspectral imaging to study InGaN/GaN multiple quantum well (MQW) structures. Different types of trench defects with varying trench width, namely wide or narrow trenches forming closed loops and open loops, are investigated in the same hyperspectral CL measurement. A strong redshift (≈90 meV) and intensity increase of the MQW emission is demonstrated for regions enclosed by wide trenches, whereas those within narrower trenches only exhibit a small redshift (≈10 meV) and a slight reduction of intensity compared with the defect-free surrounding area. Transmission electron microscopy (TEM) showed that some trench defects consist of a raised central area, which is caused by an increase of about 40% in the thickness of the InGaN wells. The causes of the changes in luminescences are also discussed in relation to TEM results identifying the underlying structure of the defect. Understanding these defects and their emission characteristics is important for further enhancement and development of light-emitting diodes.

Keywords: trench defect, cathodoluminescence, InGaN, multiple quantum wells, scanning electron microscopy

(Some figures may appear in colour only in the online journal)

1. Introduction

$In_xGa_{1-x}N$/GaN multiple quantum well (MQW) structures are the building blocks of optoelectronic devices such as light-emitting diodes (LEDs) and laser diodes [1, 2]. The advancement of the blue LED over the last few years has opened up a multi-billion dollar market for solid-state lighting, which is predicted to largely replace conventional light sources in the near future [3, 4]. However, materials within the III-nitride alloy system suffer from a wide number of defects, including compositional fluctuations [5], threading dislocations (TDs) [6], misfit dislocations [7], stacking faults [8], grain boundaries [9] and V-defects [10]. The structural and optical quality of these structures is strongly dependent on the growth conditions and the choice of substrates. One essential parameter is the growth temperature, as it is used to control the incorporation of InN (which has a low miscibility in GaN). In order to avoid decomposition of the InGaN well, the GaN barrier layers separating the InGaN quantum wells (QWs) are grown at much lower temperatures than normally used for high quality GaN films [11–13]. Furthermore, the large lattice mismatches between GaN, InN and the sapphire

substrate, and the difference in thermal expansion coefficients between GaN and the substrate, also lead to the formation of a high density of defects [14]. However, one type of defect has only been studied by a small number of groups despite its existence being well-known amongst growers and its strong impact on the luminescence: the trench-like feature or trench defect [15–21].

In this letter, we use cathodoluminescence (CL) spectroscopy to demonstrate that the trench defects can be categorized into several different types and use hyperspectral images encompassing multiple, different trenches to compare their luminescence properties. In particular we investigate the influence of the trench width on the emission properties. Cross-section transmission electron microscopy (TEM) allows us to further characterize the structural modifications caused by the trench defect and relate them to their luminescence characteristics.

2. Experimental section

The investigated InGaN/GaN MQW structures were grown by metal-organic vapour phase epitaxy. After a thick undoped low-defect-density GaN layer (TD density $\approx 4 \times 10^8\,\mathrm{cm}^{-2}$) and a 200 nm thick n-doped GaN layer, a five- or ten-period InGaN/GaN structure was deposited with nominally 2.5 nm thick wells and 7.5 nm thick barriers. The peak emission from the MQW structure is around 460 nm and the InN content in the wells was estimated to be about 17% by x-ray diffraction. To investigate the surface morphology, we used a field emission gun scanning electron microscope, equipped with a custom-built CL spectroscopy system. CL is a useful characterization tool for probing and mapping the luminescence properties of light-emitting materials, such as semiconductors [22–24]. Room temperature CL hyperspectral imaging was performed by scanning the electron beam over the sample surface and acquiring an entire luminescence spectrum at each point with a high spatial resolution approaching 10 nm [18, 25]. After data acquisition, peaks can be fitted to each constituent spectrum, and the resulting fitting parameters (e.g. peak position, intensity, width etc) plotted to create two-dimensional images which map variations in the emission characteristics. A detailed description of the CL system can be found in [25, 26]. Specimens were prepared for TEM by mechanical back-thinning and ion milling to perforation, and imaging was performed in scanning TEM mode using a high angle annular dark field (HAADF) detector.

3. Results and discussion

Secondary electron (SE) imaging revealed the presence of a high density of trench defects besides the commonly occurring V-defect. A closer look shows differences in the appearance of such defects, which enclose regions with diameter of a few 100 nm, a length scale which presents a challenge when imaging their optical properties. We identify and classify *three* types of trench defects as seen in figures 1(*a*)–(*c*): (i) *narrow* trenches forming closed loops, (ii) *wide* trenches forming closed loops and (iii) trenches forming *open* loops. These

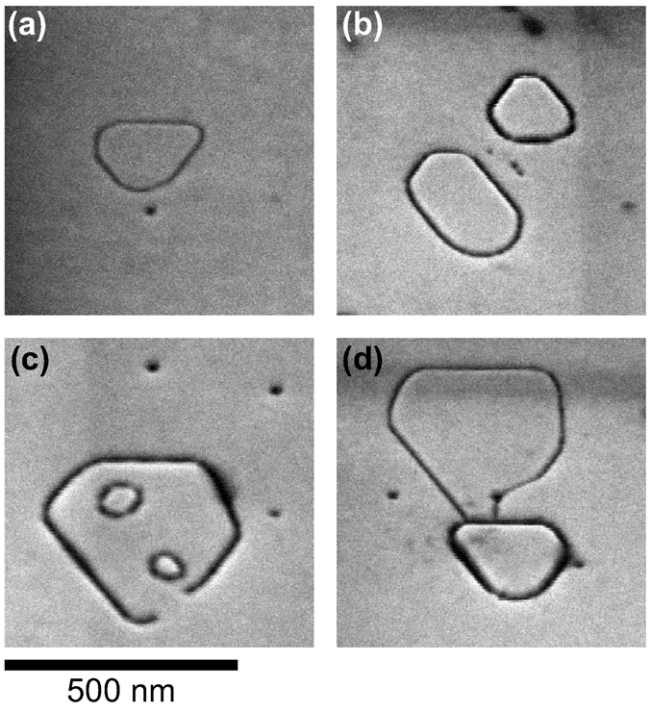

Figure 1. SE images of three different types of trench defects on the surface of a five-period InGaN/GaN MQW structure: (*a*) narrow trench forming a closed loop, (*b*) two wide trenches forming a closed loop, (*c*) open loop and (*d*) a narrow trench loop connecting a wide trench loop. The pits are V-defects, a commonly occurring defect in these kinds of structures.

three types sometimes connect with—or intersect—trenches of another kind (figure 1(*d*)) or V-defects. The trench width, of a given defect, is approximately constant around the entirety of the loop. The total trench defect density for the five-period InGaN/GaN MQW structure is approximately $1 \times 10^8\,\mathrm{cm}^{-2}$.

The luminescence behaviour of these defects is notably different from the observations on comparable structures from another growth facility as reported in [18]. In that report, CL hyperspectral imaging revealed a redshift and strong intensity increase in the luminescence from within the trench loops in comparison with the surrounding area. In contrast, the current samples are governed by trench defects of more diverse types, each having a different impact on the luminescence. Figure 2(*a*) shows an SE image containing multiple different trench defects, including (from left to right): a narrow trench loop; a wide trench loop; and interconnected narrow trench loops with an open loop. We performed CL hyperspectral imaging on this area using an acceleration voltage of 5 kV, a beam current of 100 pA, a step size of 10 nm and an exposure time of 50 ms per spectrum. From this data set, we can generate a conventional panchromatic (i.e. spectrally integrated) CL intensity image as seen in figure 2(*b*). Three distinct luminescence behaviours are observed in this intensity map. The area inside the middle defect, a wide trench loop labelled '3', exhibits a much stronger CL intensity than the regions enclosed by adjacent loops or surrounding area. These structures therefore match the trench-like feature in [18]. In contrast, the current samples also show narrower trench loops (labelled '2', '4', and '5'), which show a reduced intensity

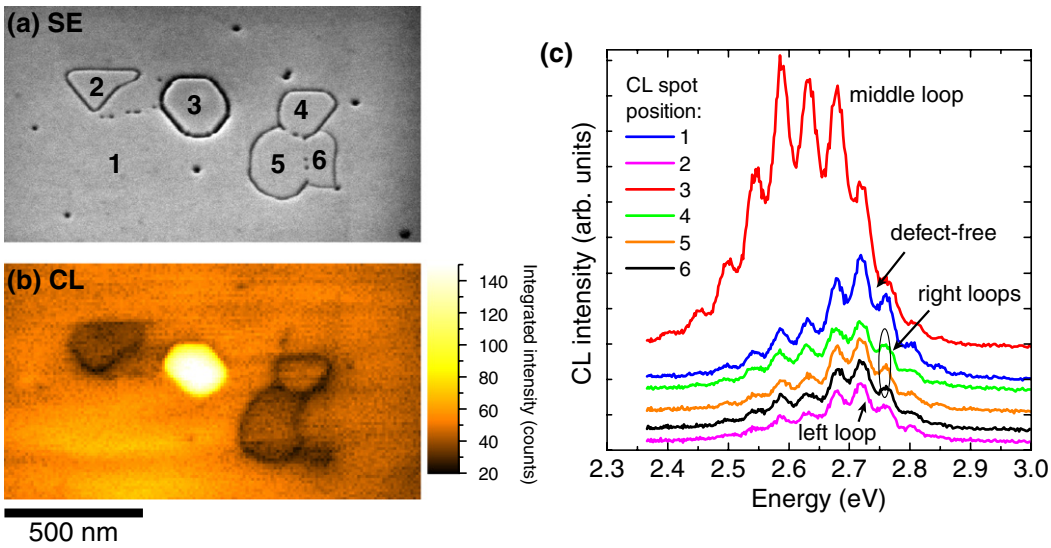

Figure 2. (*a*) SE image of three trench defects neighbouring each other, (*b*) panchromatic CL image of the same area as seen in the SE image and (*c*) CL spot spectra from six marked spots in the SE image. The spectra are offset for clarity.

compared with the trench-enclosed regions. Furthermore, there are some regions within narrow trench loops, such as 6, which display no CL intensity contrast at all. Additionally, instances of the well-known V-pits are observed, which act as centres for non-radiative recombination and therefore appear as dark spots in the CL intensity map. To further clarify this varying emission within the trench defects, we have calculated mean spectra for 5-by-5 pixel areas at six different positions, marked by numbers on the SE image in figure 2(*a*); these spectra are plotted in figure 2(*c*). The CL spectra exhibit strong thickness fringes which result from interference between the directly emitted light and that reflected from the GaN–sapphire interface. We note that the appearance of fringes is quite sensitive to the CL collection geometry. The current system collects the light from a small solid angle due to the use of a reflecting objective with a small numerical aperture and its optical axis perpendicular to the electron beam [26, 25]. In contrast, the CL spectra presented in [20, 21] are angle-integrated by a paraboloidal mirror which collects the light over a large solid angle. Region 3 shows not only a clear increase in intensity but also a redshift in its emission wavelength in comparison with the other trench defects and the surrounding (defect-free) area. Measurements on the other four positions inside the left and right trench defects show only a slight intensity reduction and small peak energy shifts compared with the defect-free area. The CL peaks also exhibit significant skew, consistent with the presence of (unresolved) longitudinal optical phonon replicas on the low energy side of the MQW emission.

Exploiting the hyperspectral nature of the CL dataset, we numerically fitted the MQW emission peak in each spectrum with a Gaussian function (taking the presence of phonon replicas into account). The resulting maps of the fitted integrated intensity and peak energy are displayed in figures 3(*a*) and (*b*), respectively. The CL intensity map from peak fitting is almost identical to the panchromatic CL image in figure 2(*b*). The CL peak energy map (figure 3(*b*)) clarifies the mean energy shifts. The area within the middle trench defect (region 3) is redshifted by about 90 meV compared with the defect-free surrounding region, while its intensity changes by almost an order of magnitude. On the other hand, the enclosed region of the narrower trench defects (regions 2, 4, and 5) only shows a small redshift of about 10 meV and a slight reduction in the intensity. As already seen in the panchromatic CL image, the area where loop 6 is located exhibits no change in the CL intensity map. Also, no energy shift is observed for region 6, whose presence appears to have no impact on the luminescence. Figure 3(*c*) shows the energy shift plotted against the width of the trenches, showing a generally increasing redshift with increasing trench width. The trenches appear as an inverse peak in an intensity line scan taken across a defect in an SE image, where the SE signal is reduced. The trench width was estimated at the points where the SE signal approached a nearly constant value on either side of the reduced signal.

While the CL data alone cannot unambiguously identify the mechanism behind the observed luminescence behaviour, when taken together with structural measurements it is possible to gain further insights into the origin of the trench defect emission. We therefore investigate the underlying structural properties of the trench defects by performing cross-section TEM measurements on a ten-period QW sample, which is in all other respects identical to the five-period QW sample [19]. A HAADF image of a sectioned trench defect is shown in figure 4, with the InGaN QWs appearing as bright line contrast due to the higher atomic number of indium in comparison with gallium. The defect bounded by two sectioned regions of the trench, indicated by white arrows, encloses a raised central area. The shadow image of a second trench very close to the first is visible due to the projection of the sectioned trench through the entire thickness of the TEM specimen. This shadow image confirms that the trenches are not V-defects, as these are pyramidal features which do not produce a shadow V-shape when viewed in cross-section. HAADF imaging of

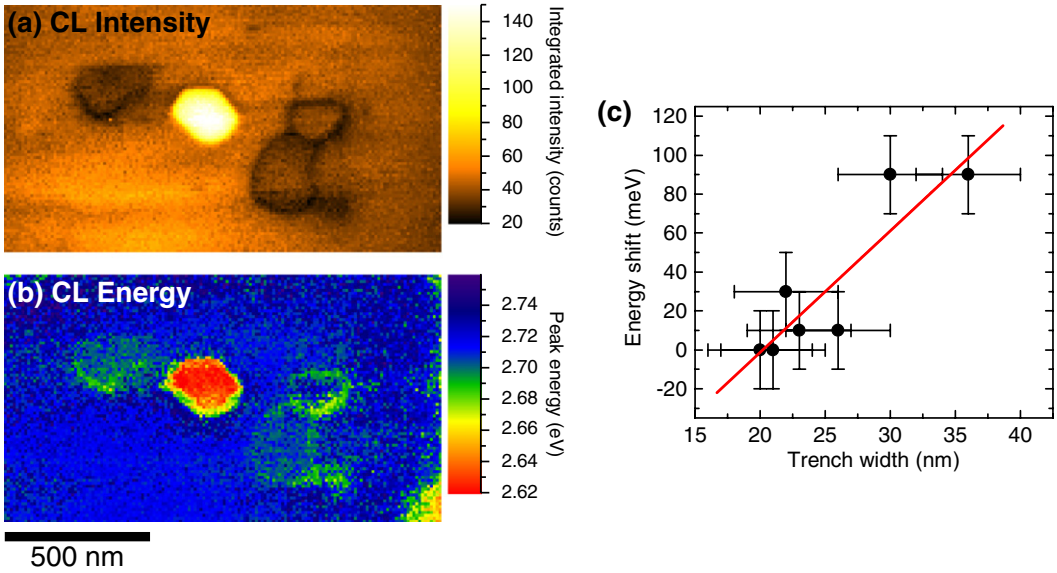

Figure 3. Room temperature CL maps gained by fitting the MQW emission peak in the hyperspectral data set with a Gaussian function: (*a*) integrated intensity and (*b*) peak energy map. (*c*) Energy shift of the inside region with respect to the surrounding area against trench width. The red line is a guide for the eye.

the defect-free area shows that the QWs and barriers are highly uniform with thicknesses of (2.5 ± 0.3) nm and (7.5 ± 0.3) nm respectively. The QWs within the enclosed region of the trench defect, however, are thicker, with an average thickness of (3.5 ± 0.3) nm, leading to the area being raised compared with the surrounding region. This confirms that the investigated samples exhibit trench defects with increased QW thickness within the enclosed region as previously observed [19].

The authors of [20] have performed further high resolution TEM investigations on these structures. It was found that a basal plane stacking fault (BSF) extends underneath the trench defect, which is connected to a vertical stacking mismatch boundary (SMB) terminated at the apex of the V-shaped trenches on either side. Straight boundaries of the defect are orientated at 60° or 120° to each other and follow $\langle 1\,\bar{1}\,0\,0 \rangle$ directions. It is proposed that whenever a change in orientation occurs the SMB opens up into a pit. Jagged sections appear where the boundary undergoes frequent changes in direction to maintain the $\langle 1\,\bar{1}\,0\,0 \rangle$ orientation of the SMB and the generated pits join to form a trench.

Ting *et al* have used atomic force microscopy (AFM) to study the surface morphology of what they called inclusions, described as larger filled-in V-pits, similar in appearance to the trench defect [15]. They reported that some of these features have an increased height of up to 12 nm. Florescu *et al* described these inclusions appearing as variously bright and dark in panchromatic CL images [16]. Both Florescu and Ting suggested that the brighter inclusions originate at the first InGaN–GaN interface, where the growth mode changes from three-dimensional island-like to two-dimensional step-flow growth. They suggest that inclusions of segregated indium or InN-rich InGaN are nucleated at those positions where TDs or V-pits intersect the InGaN–GaN interface. Further investigation by Kumar *et al* showed that the use of trimethylindium pre-flow before the InGaN well and high temperatures for the GaN barrier growth encouraged appearance of the inclusions. The additional In atoms might nucleate at V-pits and form InN-rich clusters at the GaN interface, which act as sinks for further In segregation causing the inclusions to appear during the subsequent layer growth [27]. The appearance of inclusions can be reduced or prevented by using elevated temperatures or introducing hydrogen during the GaN barrier growth, or by reducing the InGaN growth rate [15, 16, 28]. Statistical analysis of a large number of trench defects was performed by the authors of [21] linking their geometrical properties, such as trench width, area and prominence (height) of the enclosed material to their emission characteristics. For example, they demonstrate a weak correlation between prominence and redshift and almost no correlation between prominence and emission intensity.

This work studies the luminescence from trench defects of different types located side by side within a small region as seen in figure 3, with marked changes to the behaviour of the QWs and links it to structural information gained by TEM imaging as discussed in the following paragraphs. First we consider possible causes for the changes in energy and intensity seen in the CL data: (i) change in the well width; (ii) change in the InGaN composition; (iii) change in the strain state; and (iv) change in the strength of the quantum-confined Stark effect (QCSE). Several of these factors are interrelated. Possible causes of a redshift will now be considered, along with the impact on luminescence intensity. Thicker QWs could be a cause, but would be expected to lead to a decrease in intensity as the QCSE increases due to greater spatial separation between electron and hole wave functions. This enhancement of the QCSE additionally redshifts the emission. Another possibility for a redshift is an increase in the InN content, which also reduces the emission intensity due to the degradation of crystal quality. Strain relaxation has an influence on several parameters. The MQW structures are usually under compressive strain due to the pseudomorphic growth, and partial relaxation of this strain causes the emission

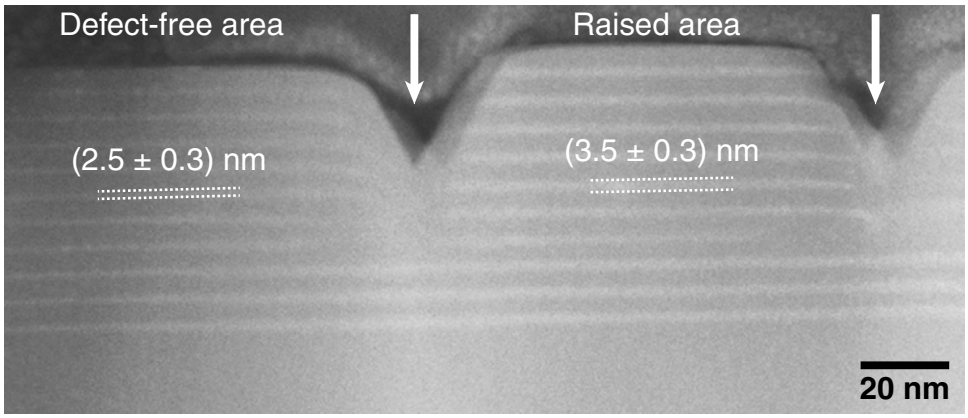

Figure 4. HAADF image of a sectioned raised trench defect of a ten-period InGaN/GaN MQW structure, with trenches indicated by arrows. The thickness of the InGaN QWs is indicated by dotted lines.

to shift to lower energies. Since strain leads to the QCSE, its reduction also results in a blueshift and increase in intensity. Strain relaxation can also cause an increase in the InN fraction through the compositional pulling effect. This has been observed in InGaN epilayers in which the gradual relaxation of strain with increasing film thickness leads to higher InN incorporation towards the top of the epilayer [29]; similar results have been found for InGaN MQWs [30]. The formation of stacking faults and the generation of V-pits by SMBs, which has been reported in [20] for the samples investigated, is one route to strain relaxation [31, 32]. A significant enhancement of the emission intensity can be due to a localization effect in the MQW region. This can be caused by potential fluctuations, such as local changes in the InN composition or well/barrier widths. An increased InN content can be related to InN-rich clusters or quantum-dot-like states within the well layer, which would also explain the strong redshift in the emission energy [33]. This makes localization in combination with one of the other effects the strongest contender to explain a redshift accompanied by an increased emission intensity (as in region 3) since most of the single effects causing an increased intensity lead to a blueshift of the emission, as described above. A combination of the above-mentioned effects, however, could lead to a redshift and significantly increased intensity, such as strain relaxation enhancing InN incorporation and leading to carrier localization. The redshift due to the InN increase and localization, however, must dominate over any blueshift from a reduced QCSE caused by relaxation in this case.

We now consider the structural information gained from TEM measurements alongside the CL results. The observed, significant variations in luminescence between the trench defects with different trench widths might be caused by different material properties within the loops, and the effect of these properties on the QWs. Considering the greater trench width of some of the loops, it is a fair assumption that with increasing width the V-shaped trenches penetrate further into the MQW structure, maybe even as far as the first QW interface. Also, the TEM findings that a vertical SMB is connected to the apex of the trench and linked to a BSF extending below the loop suggests that the affected area of the defect is separated from the surrounding material and the undisturbed QWs below the BSF. This separation could lead to altered growth conditions in the affected area causing a change in the material properties. Loops with narrower trenches might be less affected since a smaller area is altered compared with wider trenches, which penetrate further into the material.

As the HAADF image in figure 4 shows, some defects enclose QWs with increased thickness leading to that area being raised compared with the surrounding region. Thicker QWs decrease the emission energy due to weaker quantum confinement and stronger QCSE, which also decreases the emission intensity. This would agree with the observed behaviour for the defects with narrow trenches (e.g. regions 2, 4 and 5 in figure 3). Furthermore, AFM imaging on these structures showed that trench defects can have lowered, level or raised central regions [19, 20, 21]. An increase in well thickness, however, would not explain the drastic increase in intensity for the loops with wider trenches or the appearance of trench defects with level or lowered central regions since there is no additional material within the enclosed area. The correlations involving the prominence reported in [21] are also important in this respect and an alternative explanation is necessary in such cases.

The trenches themselves appear as dark lines in the CL intensity maps in figures 2(*b*) and 3(*a*). TDs generating V-pits are considered to be centres for non-radiative recombination; since TEM measurements showed the trenches consist of coalesced pits, which are caused by SMBs opening up, it is reasonable to assume that SMBs themselves also act as non-radiative recombination centres.

4. Conclusion

In summary, we have used CL hyperspectral imaging to investigate the luminescence behaviour of different types of trench defects on the surface of InGaN/GaN MQW structures. Results from CL images suggest a dependence of the emission properties of this defect on the width of the trench. While the area enclosed by wider trench defects gives luminescence which is redshifted and more intense, the emission from inside loops with narrower trenches is only slightly redshifted and its intensity is lower compared with the surrounding region. TEM measurements showed an increase in QW thickness for

the enclosed area. The observed luminescence changes could be caused by different effects and combinations of effects: thicker QWs; increased InN composition; strain relaxation (formation of SMBs and BSFs); and carrier localization (potential fluctuations or InN rich clusters). With increasing depth and width of the trenches more enclosed material is affected by the defect, effectively separating the inside region from the surrounding. For wider trench defects we propose that carrier localization dominates over other effects, whereas for narrower trench defects localizations seems to be weaker and the increased width of the QWs governs the emission properties. Deeper understanding of these defects, because of their different emission characteristics compared with the rest of the sample surface, is important for further enhancement and development of ultra-efficient LEDs based on InGaN/GaN QW structures.

Acknowledgments

We would like to thank Dr Carol Trager-Cowan and Dr Ben Hourahine for fruitful discussions, and are grateful for the financial support of the UK EPSRC (Grant Nos EP/I012591/1, EP/H004157/1 and EP/IO29141/1) and the University of Strathclyde. Access to the data underpinning the research published in their paper can be requested by contacting the corresponding author.

References

[1] Nakamura S, Mukai T and Senoh M 1994 *Appl. Phys. Lett.* **64** 1687
[2] Nakamura S, Senoh M, Nagahama S, Iwasa N, Yamada T, Matsushita T, Kiyoku H and Sugimoto Y 1996 *Japan. J. Appl. Phys.* **35** L74
[3] Schubert E F and Kim J K 2005 *Science* **308** 1274
[4] Nakamura S and Krames M 2013 *Proc. IEEE* **101** 2211
[5] Lin Y-S, Ma K-J, Hsu C, Feng S-W, Cheng Y-C, Liao C-C, Yang C-C, Chou C-C, Lee C-M and Chyi J-I 2000 *Appl. Phys. Lett.* **77** 2988
[6] Speck J and Rosner S 1999 *Physica* B **273–274** 24
[7] Costa P M F J, Datta R, Kappers M J, Vickers M E, Humphreys C J, Graham D M, Dawson P, Godfrey M J, Thrush E J and Mullins J T 2006 *Phys. Status Solidi* a **203** 1729
[8] Cho H K, Lee J Y, Kim C S, Yang G M, Sharma N and Humphreys C 2001 *J. Cryst. Growth* **231** 466
[9] Metzger T *et al* 1998 *Phil. Mag.* A **77** 1013
[10] Chen Y, Takeuchi T, Amano H, Akasaki I, Yamada N, Kaneko Y and Wang S Y 1998 *Appl. Phys. Lett.* **72** 710
[11] Thrush E J, Kappers M J, Dawson P, Graham D, Barnard J S, Vickers M E, Considine L, Mullins J T and Humphreys C J 2002 *Phys. Status Solidi* a **192** 354
[12] Pendlebury S T, Parbrook P J, Mowbray D J, Wood D A and Lee K B 2007 *J. Cryst. Growth* **307** 363
[13] Leem S J, Shin Y C, Kim E H, Kim C M, Lee B G, Moon Y, Lee I H and Kim T G 2008 *Semicond. Sci. Technol.* **23** 125039
[14] Leszczynski M *et al* 1996 *Appl. Phys. Lett.* **69** 73
[15] Ting S M *et al* 2003 *J. Appl. Phys.* **94** 1461
[16] Florescu D I, Ting S M, Ramer J C, Lee D S, Merai V N, Parkeh A, Lu D, Armour E A and Chernyak L 2003 *Appl. Phys. Lett.* **83** 33
[17] Kumar M S, Park J Y, Lee Y S, Chung S J, Hong C-H and Suh E-K 2007 *J. Phys. D: Appl. Phys.* **40** 5050
[18] Bruckbauer J, Edwards P R, Wang T and Martin R W 2011 *Appl. Phys. Lett.* **98** 141908
[19] Sahonta S-L, Kappers M J, Zhu D, Puchtler T J, Zhu T, Bennett S E, Humphreys C J and Oliver R A 2012 *Phys. Status Solidi* a **210** 195
[20] Massabuau F C-P, Sahonta S-L, Trinh-Xuan L, Rhode S, Puchtler T J, Kappers M J, Humphreys C J and Oliver R A 2012 *Appl. Phys. Lett.* **101** 212107
[21] Massabuau F C-P, Trinh-Xuan L, Lodié D, Thrush E J, Zhu D, Oehler F, Zhu T, Kappers M J, Humphreys C J and Oliver R A 2013 *J. Appl. Phys.* **113** 073505
[22] Christen J, Grundmann M and Bimberg D 1991 *J. Vac. Sci. Technol.* B **9** 2358
[23] Gustafsson A, Pistol M-E, Montelius L and Samuelson L 1998 *J. Appl. Phys.* **84** 1715
[24] Martin R W, Edwards P R, O'Donnell K P, Dawson M D, Jeon C-W, Liu C, Rice G R and Watson I M 2004 *Phys. Status Solidi* a **201** 665
[25] Edwards P R, Jagadamma L K, Bruckbauer J, Liu C, Shields P, Allsopp D, Wang T and Martin R W 2012 *Microsc. Microanal.* **18** 1212
[26] Edwards P R and Martin R W 2011 *Semicond. Sci. Technol.* **26** 064005
[27] Kumar M S, Lee Y, Park J, Chung S, Hong C-H and Suh E-K 2009 *Mater. Chem. Phys.* **113** 192
[28] Hikosaka T, Shioda T, Harada Y, Tachibana K, Sugiyama N and Nunoue S-y 2011 *Phys. Status Solidi* c **8** 2016
[29] Pereira S, Correia M R, Pereira E, O'Donnell K P, Alves E, Sequeira A D, Franco N, Watson I M and Deatcher C J 2002 *Appl. Phys. Lett.* **80** 3913
[30] Hao M, Ishikawa H, Egawa T, Shao C L and Jimbo T 2003 *Appl. Phys. Lett.* **82** 4702
[31] Cho H K, Lee J Y, Yang G M and Kim C S 2001 *Appl. Phys. Lett.* **79** 215
[32] Song T L 2005 *J. Appl. Phys.* **98** 084906
[33] O'Donnell K P, Martin R W and Middleton P G 1999 *Phys. Rev. Lett.* **82** 237